

Phase controlled single photon transport in giant atoms coupling to one-dimensional waveguide

Yan-Yan Song(宋艳艳), Yao Zang(臧耀), Yunning Lu(路云宁), Zhao Liu(刘兆), Xiao-San Ma(马小三), and Mu-Tian Cheng(程木田)

Citation: Chin. Phys. B, 2025, 34 (**12**): 124206. DOI: 10.1088/1674-1056/ade8df
http://cpb.iphy.ac.cn; http://iopscience.iop.org/cpb

What follows is a list of articles you may be interested in

Euler-modified pulley-type microring on lithium niobate platform

Wen-Hui Song(宋文慧), Dong-Jie Guo(郭东洁), Ran Yang(杨然), Jia-Chen Duan(端家晨), Zi-Shuo Gu(顾子硕), Ji Tang(汤济), Zhilin Ye(叶志霖), Xiao-Hui Tian(田晓慧), Kunpeng Jia(贾琨鹏), Zhong Yan(严仲), Zhijun Yin(尹志军), Yan-Xiao Gong(龚彦晓), Zhenda Xie(谢臻达), Zhenlin Wang(王振林), and Shi-Ning Zhu(祝世宁)

Chin. Phys. B, 2025, 34 (**8**): 084205. DOI: 10.1088/1674-1056/adee8b

Heterogeneous integration of silicon nitride photonics and CVD-grown WS_2 for second harmonic generation

Xuhang Jia(贾旭航), Bangren Xu(许邦仁), Jieyi Luo(罗劼叙), Ning Liu(刘宁), Yuhang Wang(王宇航), Biyuan Zheng(郑弼元), Wei Xu(徐威), and Ken Liu(刘肯)

Chin. Phys. B, 2025, 34 (**7**): 074205. DOI: 10.1088/1674-1056/adc7f7

Guiding and magneto-optical properties of TGG waveguide by proton implantation combined with femtosecond laser ablation

Chun-Xiao Liu(刘春晓), Zi-Hao Wang(王子昊), Bei-Er Guo(郭贝尔), Rui Yuan(袁睿), Yi-Fan Wang(王逸凡), Yu-Hang Zhou(周雨航), Jia-Bin Sun(孙家彬), Liao-Lin Zhang(张料林), and Hai-Tao Guo(郭海涛)

Chin. Phys. B, 2025, 34 (**5**): 054207. DOI: 10.1088/1674-1056/adb9cc

Experimental demonstration of silicon nitride waveguide gratings with excellent efficiency and divergence angle

Zhaozhen Chen(陈兆震), Wenling Li(李文玲), Qian Wang(王乾), Enfeng Liu(刘恩峰), Xinqun Zhang(张新群), Jingwei Liu(刘敬伟), and Zhengsheng Han(韩郑生)

Chin. Phys. B, 2025, 34 (**5**): 054206. DOI: 10.1088/1674-1056/adbbbf

Quantitative determination of modal photon number density spectrum in arbitrary dielectric structures with a quantum emitter

Li-Heng Chen(陈立恒), Fengfeng Luo(罗凤凤), and Yonggui Gao(高勇贵)

Chin. Phys. B, 2025, 34 (**4**): 044204. DOI: 10.1088/1674-1056/adb262

Phase controlled single photon transport in giant atoms coupling to one-dimensional waveguide

Yan-Yan Song(宋艳艳)[1], Yao Zang(臧耀)[1], Yunning Lu(路云宁)[1], Zhao Liu(刘兆)[1], Xiao-San Ma(马小三)[1,2], and Mu-Tian Cheng(程木田)[1,2,†]

[1] *School of Electrical Engineering & Information, Anhui University of Technology, Maanshan* 243002, *China*
[2] *Anhui Provincial Key Laboratory of Power Electronics & Motion Control, Anhui University of Technology, Maanshan* 243002, *China*

(Received 6 April 2025; revised manuscript received 4 June 2025; accepted manuscript online 27 June 2025)

The phase-controlled single-photon transport properties of a giant atom coupled to a one-dimensional waveguide are investigated. The coupling between the giant atom and the waveguide is modeled as a multi-point interaction. The coupling strengths between the giant atom and the waveguide are represented as complex numbers with associated phases. Analytical expressions for the scattering amplitudes are obtained using the real-space Hamiltonian method. The results show that the characteristics of the scattering spectra, including the positions of peaks (or dips) and the full width at half maximum, can be tuned by adjusting the phase difference between the coupling strengths. Further calculations reveal that the scattering spectra can be either super-broadened or sub-broadened. The conditions for achieving perfect nonreciprocal single-photon transport in the Markovian regime are also discussed. Moreover, we demonstrate the control of single-photon transport through phase differences in the non-Markovian regime. Our results may find applications in the design of quantum devices operating at the single-photon level, based on waveguide quantum electrodynamics.

Keywords: giant atom, waveguide, nonreciprocal single photon scattering

PACS: 42.50.Nn, 42.50.Ct, 32.70.Jz

DOI: 10.1088/1674-1056/ade8df **CSTR:** 32038.14.CPB.ade8df

1. Introduction

Waveguide quantum electrodynamics, which studies the interactions between quantum emitters and propagating photons in waveguides, has attracted much attention due to its potential applications in quantum information processing,[1–3] quantum computing,[4–7] and as a promising platform[8,9] for investigating quantum optical phenomena. Generally, most quantum emitters, such as atoms, quantum dots, and NV centers, can be regarded as point-like because their sizes are negligible compared to the wavelength of the field.[10,11] Recently, interactions between superconducting qubits coupled to acoustic waves or microwave waveguides have been reported.[12–15] Different from the case of small atoms with single-point coupling, the coupling between superconducting qubits and acoustic waves should be treated as multi-point coupling, since the size of the qubit is comparable to the wavelength of the photon propagating in the waveguide. The multi-point coupling introduces new interaction pathways between the emitter and the waveguide, leading to many interesting results.[16–23] These studies provide new methods for designing quantum devices and offer a platform to explore various quantum effects, such as decoherence-free subspaces,[24,25] frequency-comb emission,[26] bound states,[27,28] and the Lamb shift.[29]

Single-photon scattering by giant atoms coupled to a one-dimensional waveguide has become a hot topic in constructing quantum networks. Wang *et al.*[30] reported single-photon scattering properties in a hybrid system composed of giant atoms interacting with a coupled-resonator waveguide through two or multiple coupling points. Subsequently, several groups investigated single-photon scattering in different configurations, including giant atoms interacting with waveguides exhibiting linear dispersion relations,[31–33] nonlinear dispersion relations,[34,35] or topological properties,[36–38] as well as multiple giant atoms coupled to waveguides,[39,40] etc. These investigations provide many approaches to control single-photon scattering. Based on these results, various quantum devices, such as quantum routers[41–44] and frequency converters,[45] have been proposed.

The phases of the coupling strengths between quantum emitters and the waveguide are often neglected in many models. However, when the number of interaction channels between emitters and the waveguide is no less than two, the phase differences between the coupling strengths may play an important role in manipulating quantum phenomena due to quantum interference effects. We have previously studied phase-controlled single-photon routing between two waveguides.[46] Recent reports show that single-photon nonreciprocal transport can be realized by manipulating the phase differences between coupling strengths arising from the multi-point coupling between giant atoms and the waveguide.[47] The phase difference, together with energy dissipation, leads to chiral coupling between the giant atom and the waveg-

†Corresponding author. E-mail: mtcheng@ahut.edu.cn

© 2025 Chinese Physical Society and IOP Publishing Ltd. All rights, including for text and data mining, AI training, and similar technologies, are reserved.

uide. Subsequently, several papers reported the realization of nonreciprocal single-photon scattering based on the coupling between giant atoms and waveguides.[35,48–55] Many quantum devices, including quantum routers[41,42] and frequency-tunable single-photon diodes,[56] have been proposed. However, most of these results are based on the two-point coupling model. Multi-point coupling can provide additional interaction channels between the giant atom and the waveguide, allowing the system to exhibit richer physical phenomena. For example, it can produce broad photonic band gaps.[57] The steady-state entanglement between two giant atoms can also be enhanced by increasing the number of coupling points.[58] Recently, Xu and Guo[59] investigated chirality, nonreciprocity, and symmetries for a giant atom with multi-point coupling. Here, we further investigate phase-controlled single-photon transport in a giant-atom–waveguide system. We show that the full width at half maximum (FWHM) of the scattering spectra and the positions of the peaks can be well controlled by the phase differences between the coupling strengths. The conditions for realizing perfect nonreciprocity in the transmission spectra are also analyzed. Furthermore, we show that the single-photon scattering spectra can be strongly affected by the time delay induced by photon propagation.

2. Model and Hamiltonian of the system

The system considered in this paper is shown in Fig. 1. A giant atom with an excited state $|e\rangle$ and a ground state $|g\rangle$ is coupled to a waveguide at positions $x = x_m$. The coupling strengths at $x = x_m$ are denoted as $g\,\mathrm{e}^{\mathrm{i}\phi_m}$, where g is a real constant and ϕ_m represents the phase. The local coupling phases ϕ_m can be introduced through Josephson-junction loops threaded by external magnetic fluxes in superconducting quantum devices.[19]

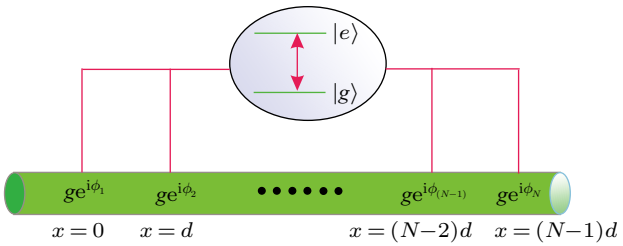


Fig. 1. Schematic diagram of the system considered in this paper. A giant atom couples to a waveguide at N equally spaced points with separation d. The coupling strength between the giant atom and the waveguide at each point is denoted as $g\,\mathrm{e}^{\mathrm{i}\phi_m}$.

Under the rotating-wave approximation, the system Hamiltonian in real space can be written as ($\hbar = 1$)

$$\begin{aligned} H_{A_x} &= (\omega_e - \mathrm{i}\gamma)\sigma_{ee} + \int \mathrm{d}x C_{\mathrm{R}}^{\dagger}(x)\left(-\mathrm{i}v_{\mathrm{g}}\frac{\partial}{\partial x}\right)C_{\mathrm{R}}(x) \\ &\quad + \int \mathrm{d}x C_{\mathrm{L}}^{\dagger}(x)\left(\mathrm{i}v_{\mathrm{g}}\frac{\partial}{\partial x}\right)C_{\mathrm{L}}(x) \\ &\quad + \sum_{m=1}^{N}\int \mathrm{d}x\, g\,\mathrm{e}^{\mathrm{i}\phi_m}\delta(x-x_m)[C_{\mathrm{R}}^{\dagger}(x)+C_{\mathrm{L}}^{\dagger}(x)]\sigma_{ge} \\ &\quad + \sum_{m=1}^{N}\int \mathrm{d}x\, g\,\mathrm{e}^{-\mathrm{i}\phi_m}\delta(x-x_m)[C_{\mathrm{R}}(x)+C_{\mathrm{L}}(x)]\sigma_{eg}. \end{aligned} \tag{1}$$

Here, ω_e is the transition frequency between $|e\rangle$ and $|g\rangle$, and 2γ represents the energy loss from $|e\rangle$ to the non-waveguide modes. $C_{\mathrm{R}}^{\dagger}(x)$ ($C_{\mathrm{L}}^{\dagger}(x)$) denotes the creation operator for a right- (left-) propagating photon in the waveguide at position x. v_{g} is the group velocity of the photon in the waveguide, $\delta(x)$ is the Dirac delta function, and σ_{ge} represents the dipole transition operator.

Since we consider only a single excitation in the system, the eigenstate of the Hamiltonian can be written as

$$\begin{aligned} |\Psi_{A_x}\rangle &= \int \mathrm{d}x\, u_{\mathrm{R}}(x)C_{\mathrm{R}}^{\dagger}(x)|0\rangle + \int \mathrm{d}x\, u_{\mathrm{L}}(x)C_{\mathrm{L}}^{\dagger}(x)|0\rangle \\ &\quad + u_e\sigma_{eg}|0\rangle, \end{aligned} \tag{2}$$

where $|0\rangle$ denotes the vacuum state with no photons in the waveguide and the giant atom in its ground state. $u_{\mathrm{R}}(x)$ ($u_{\mathrm{L}}(x)$) is the probability amplitude of the right- (left-) propagating photon in the waveguide, and u_e is the excitation probability amplitude of the giant atom.

Assuming a single photon incident from the left side of the waveguide, $u_{\mathrm{R}}(x)$ and $u_{\mathrm{L}}(x)$ are defined as

$$u_{\mathrm{R}}(x) = \begin{cases} \mathrm{e}^{\mathrm{i}kx}, & x < 0, \\ t_m\,\mathrm{e}^{\mathrm{i}k(x-md)}, & (m-1)d < x < md, \\ t_N\,\mathrm{e}^{\mathrm{i}k(x-Nd)}, & (N-1)d < x, \end{cases} \tag{3}$$

$$u_{\mathrm{L}}(x) = \begin{cases} r_1\,\mathrm{e}^{-\mathrm{i}kx}, & x < 0, \\ r_{m+1}\,\mathrm{e}^{-\mathrm{i}k(x-md)}, & (m-1)d < x < md, \\ 0, & (N-1)d < x. \end{cases} \tag{4}$$

Here, $t_m\,\mathrm{e}^{\mathrm{i}k(x-md)}$ [$r_{m+1}\,\mathrm{e}^{-\mathrm{i}k(x-md)}$] denotes the right- (left-) propagating photon in the region between x_j and x_{j+1}, and t_j and r_j are coefficients to be determined. Substituting Eqs. (3) and (4) into the Schrödinger equation $H|E_k\rangle = E_k|E_k\rangle$, we obtain

$$t_m\,\mathrm{e}^{-\mathrm{i}kd} - t_{m-1} + \mathrm{i}\frac{g\,\mathrm{e}^{\mathrm{i}\phi_m}u}{v_{\mathrm{g}}} = 0, \tag{5}$$

$$r_{m+1}\,\mathrm{e}^{\mathrm{i}kd} - r_m - \mathrm{i}\frac{g\,\mathrm{e}^{\mathrm{i}\phi_m}u}{v_{\mathrm{g}}} = 0, \tag{6}$$

$$\sum_m g\,\mathrm{e}^{-\mathrm{i}\phi_m}(t_{m-1}+r_m) - (\Delta+\mathrm{i}\gamma)u = 0, \tag{7}$$

where $\Delta = \omega - \omega_e$, and $t_0 = 1$, $r_{N+1} = 0$ are defined. The transmission and reflection coefficients of the system are given by $t_{\mathrm{l}} = t_N\,\mathrm{e}^{-\mathrm{i}kNd}$ and $r = r_1$, respectively. The subscript l denotes a single photon incident from the left of the waveguide. From Eqs. (5)–(7), after straightforward algebra, one obtains

$$t_{\mathrm{l}} = \frac{\Delta - \Delta_{\mathrm{ls}} + \mathrm{i}(\gamma - \gamma_{\mathrm{in}})}{\Delta - \Delta_{\mathrm{ls}} + \mathrm{i}(\gamma + \Gamma_{\mathrm{eff}})}, \tag{8a}$$

$$r=\frac{-\mathrm{i}\Gamma\sum\limits_{m=1}^{N}\mathrm{e}^{\mathrm{i}(m-1)\theta+\mathrm{i}(\phi_m-\phi_1)}\sum\limits_{m=1}^{N}\mathrm{e}^{\mathrm{i}(m-1)\theta-\mathrm{i}(\phi_m-\phi_1)}}{\Delta-\Delta_{\mathrm{ls}}+\mathrm{i}(\gamma+\Gamma_{\mathrm{eff}})}, \tag{8b}$$

where $\Gamma=g^2/v_{\mathrm{g}}$. The induced decay rate γ_{in}, the Lamb shift Δ_{ls}, and the effective decay rate from the giant atom to the propagating waveguide mode Γ_{eff} are given by

$$\gamma_{\mathrm{in}}=2\Gamma\sum_{m>n}^{N}[\sin(\phi_m-\phi_n)\sin((m-n)\theta)], \tag{9a}$$

$$\Delta_{\mathrm{ls}}=2\Gamma\sum_{m>n}^{N}[\cos(\phi_m-\phi_n)\sin((m-n)\theta)], \tag{9b}$$

$$\Gamma_{\mathrm{eff}}=N\Gamma+2\Gamma\sum_{m>n}^{N}[\cos(\phi_m-\phi_n)\cos((m-n)\theta)]. \tag{9c}$$

Here, θ is the accumulated phase resulting from photon propagation between two adjacent points, given by $\theta=kd=\tau(\omega_e+\Delta)=\theta_0+\tau\Delta$. $\tau=d/v_{\mathrm{g}}$ denotes the photon propagation time between adjacent points, and $\theta_0=\tau\omega_e$. When τ is small, the term $\tau\Delta$ can be neglected, and the system can be regarded as in the Markovian regime. However, when τ is large, the contribution of $\tau\Delta$ to single-photon scattering must be considered. In this case, the system enters the non-Markovian regime. It is straightforward to verify that when ϕ_m remains constant, the results reduce to those in Ref. [57].

Equations (9a)–(9c) indicate that γ_{in}, Δ_{ls}, and Γ_{eff} depend strongly on the phases of the coupling strengths. Thus, by manipulating the phases ϕ_m, one can control the single-photon scattering properties of the system. For convenience, the energy loss rate γ is neglected temporarily. We set $\phi_{m+1}-\phi_m=\phi$ in the following calculations. In this case, Eqs. (9a)–(9c) can be rewritten as

$$\gamma_{\mathrm{in}}=2\Gamma\sum_{s=1}^{N-1}[(N-s)\sin(s\phi)\sin(s\theta)], \tag{10a}$$

$$\Delta_{\mathrm{ls}}=2\Gamma\sum_{s=1}^{N-1}[(N-s)\cos(s\phi)\sin(s\theta)], \tag{10b}$$

$$\Gamma_{\mathrm{eff}}=N\Gamma+2\Gamma\sum_{s=1}^{N-1}[(N-s)\cos(s\phi)\cos(s\theta)]. \tag{10c}$$

3. Phase-controlled single-photon transport in the Markovian regime

3.1. Two-point coupling model

We first consider a two-point coupling model, corresponding to the case $\theta\approx\theta_0$. To reveal the influence of ϕ, we analyze the two-point coupling configuration based on Eqs. (8a) and (8b). The transmission and reflection amplitudes are obtained as follows:

$$t_{\mathrm{l2p}}=\frac{\Delta-2\Gamma\cos\phi\sin\theta-\mathrm{i}2\Gamma\sin\phi\sin\theta}{\Delta-2\Gamma\cos\phi\sin\theta+\mathrm{i}2\Gamma(1+\cos\phi\cos\theta)}, \tag{11a}$$

$$r_{\mathrm{2p}}=\frac{-\mathrm{i}\Gamma[1+\mathrm{e}^{\mathrm{i}(\theta+\phi)}][1+\mathrm{e}^{\mathrm{i}(\theta-\phi)}]}{\Delta-2\Gamma\cos\phi\sin\theta+\mathrm{i}2\Gamma(1+\cos\phi\cos\theta)}. \tag{11b}$$

The induced decay, Lamb shift, and effective decay rate for the two-point coupling model are given by $\gamma_{\mathrm{in}}=2\Gamma\sin\theta\sin\phi$, $\Delta_{\mathrm{ls2p}}=2\Gamma\cos\theta\cos\phi$, and $\Gamma_{\mathrm{eff2p}}=2\Gamma(1+\cos\theta\cos\phi)$, respectively. In the following, we discuss how to manipulate the single-photon scattering properties by tuning θ and ϕ.

(1) When $\theta=p\pi$, one finds that $\gamma_{\mathrm{in}}=\Delta_{\mathrm{ls2p}}=0$. The induced decay and Lamb shift vanish and are independent of ϕ in this condition. However, $\Gamma_{\mathrm{eff2p}}=2\Gamma(1+\cos\alpha)$, which is controlled by the phase ϕ, where $\alpha=p\pi-\phi$. The single-photon transmission ($T_{\mathrm{l2p}}\equiv|t_{\mathrm{l}}|^2$) and reflection ($R_{\mathrm{2p}}\equiv|r|^2$) probabilities are expressed as

$$T_{\mathrm{l2p}}=\frac{\Delta^2}{\Delta^2+[2\Gamma(1+\cos\alpha)]^2}, \tag{12a}$$

$$R_{\mathrm{2p}}=\frac{[2\Gamma(1+\cos\alpha)]^2}{\Delta^2+[2\Gamma(1+\cos\alpha)]^2}. \tag{12b}$$

It is shown that R_{2p} exhibits a standard Lorentzian lineshape centered at $\Delta=0$, with a FWHM of $4\Gamma(1+\cos\alpha)$, while T_{2p} displays an anti-Lorentzian profile. Interestingly, when $\alpha=p\pi-\phi=2n\pi$, where n is an integer, $\cos\alpha$ reaches its maximum value of 1. Consequently, $\Gamma_{\mathrm{eff2p}}=4\Gamma=2^2\Gamma$, and the FWHM of the transmission spectrum becomes 8Γ. The scattering spectra are thus superbroaded, as shown in Fig. 2(a). Conversely, when $\alpha=p\pi-\phi=(2n+1)\pi$, $\Gamma_{\mathrm{eff2p}}=0$, indicating that the giant atom effectively decouples from the waveguide due to quantum interference between the two photonic paths, resulting in $T=1$.

Figure 2 presents R_{2p} as a function of Δ and ϕ for $\theta=2\pi$ (a) and $\theta=\pi$ (b). It clearly demonstrates that the scattering spectra are symmetric with respect to Δ for fixed ϕ. This symmetry originates from the disappearance of the Lamb shift. Figures 2(e) and 2(f) show cross-sections of (a) and (b), respectively, exhibiting standard Lorentzian profiles centered at $\Delta=0$. These results indicate that the width of the scattering spectra can be strongly manipulated by controlling ϕ.

(2) When $\theta=(p+1/2)\pi$, one obtains $\gamma_{\mathrm{in}}=(-1)^p2\Gamma\sin\phi$, $\Delta_{\mathrm{ls2p}}=(-1)^p2\Gamma\cos\phi$, and $\Gamma_{\mathrm{eff2p}}=2\Gamma$. Accordingly, T_{l} and R are expressed as

$$T_{\mathrm{l2p}}=\frac{(\Delta\pm2\Gamma\cos\phi)^2+4\Gamma^2\sin^2\phi}{(\Delta\pm2\Gamma\cos\phi)^2+4\Gamma^2}, \tag{13a}$$

$$R_{\mathrm{2p}}=\frac{4\Gamma^2\cos^2\phi}{(\Delta\pm2\Gamma\cos\phi)^2+4\Gamma^2}. \tag{13b}$$

The reflection spectrum exhibits a Lorentzian profile centered at $\Delta=\mp2\Gamma\cos\phi$, with an FWHM of 8Γ. The peak value of R can be significantly tuned by adjusting ϕ. When $\phi=(p+1/2)\pi$, R vanishes and T reaches unity due to quantum interference, implying perfect transmission. For $\phi=q\pi$, where q is an even integer, R reaches its maximum value of 1 at $\Delta=2\Gamma$, while for odd q, $R=1$ occurs at $\Delta=-2\Gamma$, as shown in Figs. 2(c) and 2(d). Therefore, by adjusting ϕ and Γ, one can control the position of the reflection peak, achieving either a redshift or a blueshift in the scattering spectra.

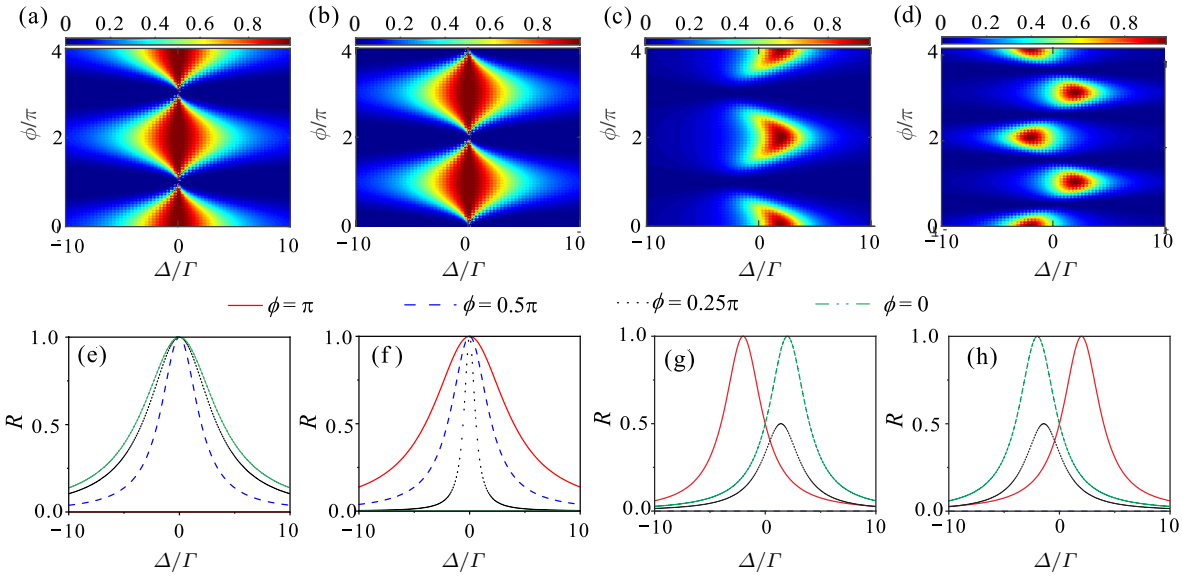


Fig. 2. Single-photon reflection spectra controlled by the phase difference ϕ between the coupling strengths for $N=2$. The calculated parameters are $\theta=2\pi$ (a), $\theta=\pi$ (b), $\theta=\pi/2$ (c), and $\theta=3\pi/2$ (d). Panels (e)–(h) are extracted from (a)–(d), respectively. In all calculations, $\Gamma=10^{-5}\omega_e$.

3.2. N-point coupling model

Equations (10c) to (20a) show that when $\theta=2p\pi$ and $\phi=2q\pi$, or $\theta=(2p+1)\pi$ and $\phi=(2q+1)\pi$, where p and q are integers, one has $\Gamma_{\rm eff}=N^2\Gamma$, which is analogous to the case of superradiance. Since the width of the scattering spectra strongly depends on $\Gamma_{\rm eff}$, this situation can thus be considered as a case of superbroadening. Furthermore, when $\theta=2p\pi$ and $\phi=2\pi/N$, $\Gamma_{\rm eff}=0$, and the incident photon transmits with unit probability. Therefore, this case can be regarded as a sub-broadening of the scattering spectra.

By substituting Eqs. (10b), (10c), and (20a) into Eqs. (8a) and (8b), one obtains the analytical expressions of the scattering probabilities for the N-point coupling model with phase-dependent coupling strengths. When $N=3$, $\theta=p\pi$, and $\Delta_{\rm ls}=\gamma_{\rm in}=0$, we have $\Gamma_{\rm eff}=\Gamma(3+2\cos\phi+\cos 2\phi)$. The reflection and transmission probabilities are given by

$$T_{\rm 3p}=\frac{\Delta^2}{\Delta^2+[\Gamma(3+2\cos\phi+\cos 2\phi)]^2}, \tag{14a}$$

$$R_{\rm 3p}=\frac{[\Gamma(3+2\cos\phi+\cos 2\phi)]^2}{\Delta^2+[\Gamma(3+2\cos\phi+\cos 2\phi)]^2}. \tag{14b}$$

The reflection spectra also show a standard Lorentzian lineshape with a FWHM of $2\Gamma_{\rm eff}$. When $\phi=2\pi$, $\Gamma_{\rm eff}=3^2\Gamma=9\Gamma$. The reflection spectra are superbroadened, as shown in Figs. 3(a) and 3(c). However, when $\phi=2\pi/3$, one obtains $\Gamma_{\rm eff}=0$, and the reflection probabilities remain zero. Thus, for the case of $\theta=2\pi$, one can control the resonant photon from being perfectly reflected to being perfectly transmitted by adjusting the phase ϕ.

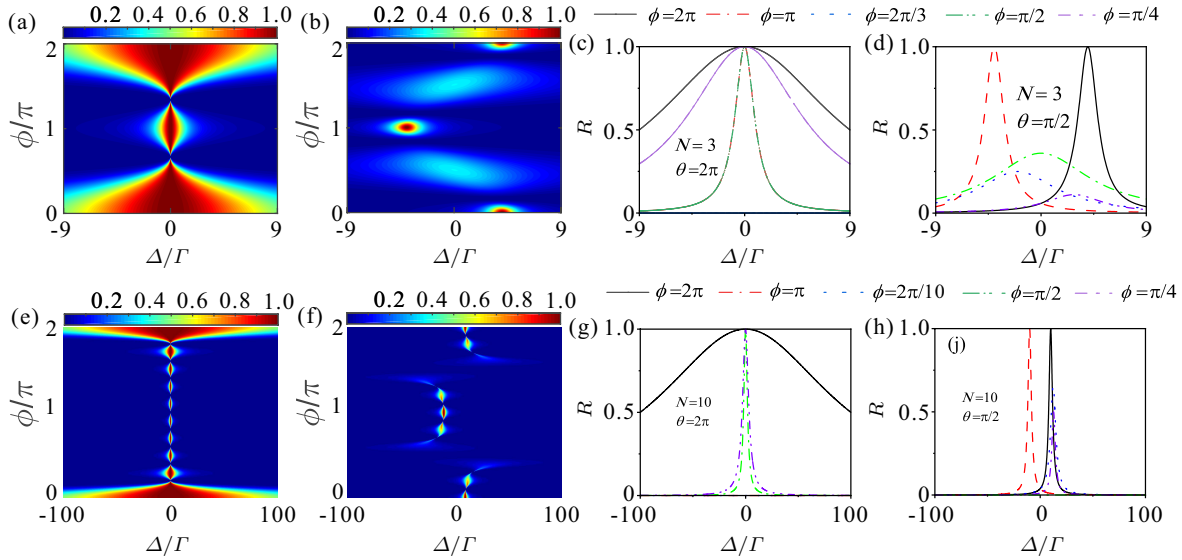


Fig. 3. Single-photon reflection spectra controlled by ϕ. In panels (a) and (b), $N=3$ with $\theta=2\pi$ and $\theta=\pi/2$, respectively. Panels (c) and (d) are extracted from panels (a) and (b), respectively. In panels (e) and (f), $N=10$ with $\theta=2\pi$ and $\theta=\pi/2$, respectively. Panels (g) and (h) are extracted from panels (e) and (f), respectively. In all calculations, $\Gamma=10^{-5}\omega_e$.

When $\theta = p\pi + \pi/2$, $\gamma_{\rm in}$, $\Delta_{\rm ls}$, and $\Gamma_{\rm eff}$ are given by $\gamma_{\rm in} = (-1)^p 4\Gamma \sin\phi$, $\Delta_{\rm ls3p} = (-1)^p 4\Gamma\cos\phi$, and $\Gamma_{\rm eff3p} = 3\Gamma + (-1)^{p+1}\cos 2\phi$. Therefore, the position of the reflection spectra at which the maximum value is reached can be controlled by tuning ϕ. When $\phi = 2\pi$, the reflection spectra reach their maximum value of 1 at $\Delta = \Delta_{\rm ls} = 4\Gamma$. However, when $\phi = \pi$, this maximum shifts to $\Delta = -4\Gamma$, as shown in Figs. 3(b) and 3(d).

When the number of coupling points increases to 10, the behavior of the scattering properties remains similar to that in the case of $N = 3$, as displayed in Figs. 3(e)–3(h). It is found that $\Gamma_{\rm eff}$ increases to $10^2\Gamma = 100\Gamma$ under the condition $\theta = \phi = 2\pi$. The FWHM of the reflection spectra is 200Γ, as shown in Figs. 3(e) and 3(g). When $\phi = 2\pi/10 = \pi/5$, $\Gamma_{\rm eff} = 0$, and the incident photon transmits freely. Thus, for $\theta = 2\pi$, the single-photon transport can be tuned continuously from full reflection to complete transmission by manipulating the phase ϕ.

4. Nonreciprocal single-photon transmission

We now discuss how to realize nonreciprocal single-photon transmission in this system. When a single photon is incident from the right side of the waveguide, the transmission amplitude $t_{\rm r}$ is given by

$$t_{\rm r} = \frac{\Delta - \Delta_{\rm ls} + {\rm i}(\gamma + \gamma_{\rm in})}{\Delta - \Delta_{\rm ls} + {\rm i}(\gamma + \Gamma_{\rm eff})}. \tag{15}$$

The corresponding transmission probability $T_{\rm r}$ is

$$T_{\rm r} = \frac{(\Delta - \Delta_{\rm ls})^2 + (\gamma + \gamma_{\rm in})^2}{(\Delta - \Delta_{\rm ls})^2 + (\gamma + \Gamma_{\rm eff})^2}. \tag{16}$$

To quantitatively describe the nonreciprocal single-photon transmission, we define $\Delta T = |T_{\rm l} - T_{\rm r}|$. When $\Delta T = 1$, perfect single-photon isolation is achieved, while $\Delta T = 0$ corresponds to reciprocal transmission. After some straightforward algebra, ΔT can be expressed as

$$\Delta T = \frac{4\gamma|\gamma_{\rm in}|}{(\Delta - \Delta_{\rm ls})^2 + (\gamma + \Gamma_{\rm eff})^2}. \tag{17}$$

It is evident that γ plays a crucial role in realizing perfect nonreciprocity. When $\gamma = 0$, ΔT always equals zero, and the nonreciprocity vanishes. Similarly, when $|\gamma_{\rm in}| = 0$, the transmission is reciprocal, implying that the nonreciprocity disappears for $\theta = p\pi$ or $\phi = p\pi$. The conditions for achieving perfect nonreciprocity can be obtained as

$$\Delta = \Delta_{\rm ls}, \tag{18a}$$

$$4\gamma|\gamma_{\rm in}| = (\gamma + \Gamma_{\rm eff})^2. \tag{18b}$$

Under these conditions, $\Delta T = 1$, and perfect nonreciprocal transmission is realized. The physical mechanism underlying this effect can be explained as follows: when the single photon is incident from one direction, it is absorbed by the atom and then re-emitted into free space, resulting in no reflection or transmission. In contrast, when the photon is incident from the opposite direction, it is transmitted with unit probability.

For the two-point coupling model, the conditions for achieving perfect nonreciprocity become $\Delta = \Delta_{\rm ls}$ and

$$8\gamma\Gamma\sin\theta\sin\phi = [\gamma + 2\Gamma(1 + \cos\theta\cos\phi)]^2, \tag{19}$$

which are consistent with previous reports. It shows that when $\theta = \phi = \pi/2$ and $\gamma = 2\Gamma$, $\Delta T = 1$ at $\Delta = 0$, indicating that perfect nonreciprocity is achieved.

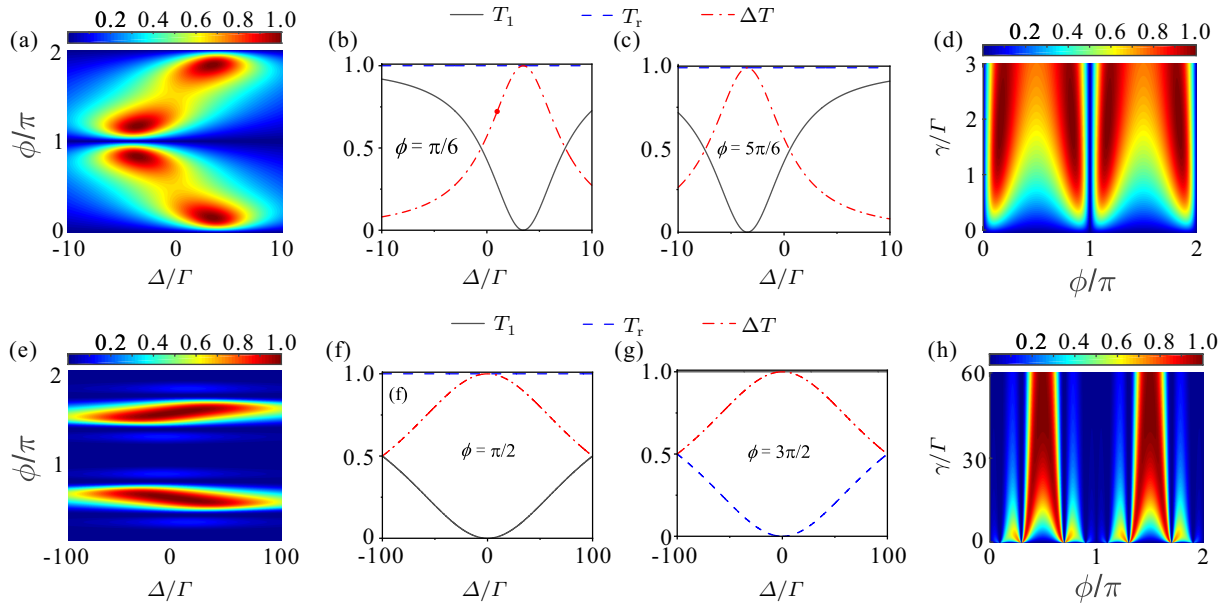


Fig. 4. Nonreciprocal single-photon scattering in the Markovian regime. Panels (a) and (e) show ΔT varying with frequency detuning Δ and γ for $N = 3$ and $N = 10$, respectively. Panels (b) and (c) are extracted from (a) at $\phi = \pi/6$ and $\phi = 5\pi/6$, respectively, with $\gamma = 2\Gamma$. Panels (f) and (g) are extracted from (e) at $\phi = \pi/2$ and $\phi = 3\pi/2$, respectively, with $\gamma = 50\Gamma$. Panels (d) and (h) show ΔT varying with ϕ and γ at $\Delta = \Delta_{\rm ls}$ for $N = 3$ and $N = 10$, respectively.

For the three-point coupling model, when $\theta = \pi/2$, $\phi = (p \pm 1/6)\pi$, and $\gamma = 2\Gamma$, one obtains $\Delta T = 1$ at $\Delta = 2\sqrt{3}\Gamma$ [for $\phi = (2p \pm 1/6)\pi$] or at $\Delta = -2\sqrt{3}\Gamma$ [for $\phi = (2p+1 \pm 1/6)\pi$]. With the increase in the number of coupling points, the corresponding values of γ and ϕ that yield perfect nonreciprocal single-photon transmission can be determined from the condition $4\gamma|\gamma_{\rm in}| = (\gamma + \Gamma_{\rm eff})^2$.

For the case of $N = 10$, it shows that $\Delta T = 1$ at $\Delta = 0$ when $\theta = \pi/2$ and $\phi = \pm\pi/2$ with $\gamma = 50\Gamma$. Figure 4 illustrates the dependence of ΔT on γ and ϕ for $N = 3$ and $N = 10$, showing that the simulated results are in excellent agreement with the theoretical analysis.

5. Phase-controlled single-photon scattering in the non-Markovian regime

When the time delay becomes significant such that the term $\tau\Delta$ cannot be neglected, the system dynamics enter the non-Markovian regime. In this regime, the single-photon scattering behavior is strongly modified, and the nonreciprocal scattering properties are also influenced by the time delay.

In the Markovian case, for $\theta = k\pi$, one always has $\Delta T = 0$ due to $\gamma_{\rm in} = 0$. However, in the non-Markovian regime, ΔT may deviate from zero as a result of the time-delay effect. This indicates that the time delay itself can induce single-photon nonreciprocity. Moreover, the degree of nonreciprocity can be further tuned by adjusting the phase difference ϕ.

The conditions for achieving perfect nonreciprocity remain $\Delta = \Delta_{\rm ls}$ and $4\gamma|\gamma_{\rm in}| = (\gamma + \Gamma_{\rm eff})^2$. However, in the non-Markovian regime, all three parameters — $\gamma_{\rm in}$, $\Delta_{\rm ls}$, and $\Gamma_{\rm eff}$ — become functions of $\tau\Delta$ and are thus modified by the time delay.

Figure 5 illustrates ΔT and the reflection spectra in the non-Markovian regime with $\tau\Gamma = \pi/4$. Both ΔT and R exhibit oscillatory behavior as functions of Δ, which is in sharp contrast to the Markovian case. For $N = 3$ and $\phi = \pi/6$, ΔT reaches its maximum at $\Delta \approx -4\Gamma$, differing from the Markovian case where the maximum occurs at $\Delta = 4\Gamma$. Therefore, in the non-Markovian regime, the conditions for perfect nonreciprocity should be determined using Eqs. (18a) and (18b).

For $N = 10$ with $\theta = \phi = \pi/2$, ΔT displays nearly periodic oscillations with respect to Δ, as shown in Fig. 5(d), with a period of approximately 4.04Γ. This property could be utilized to design single-photon diodes operating at different frequencies.

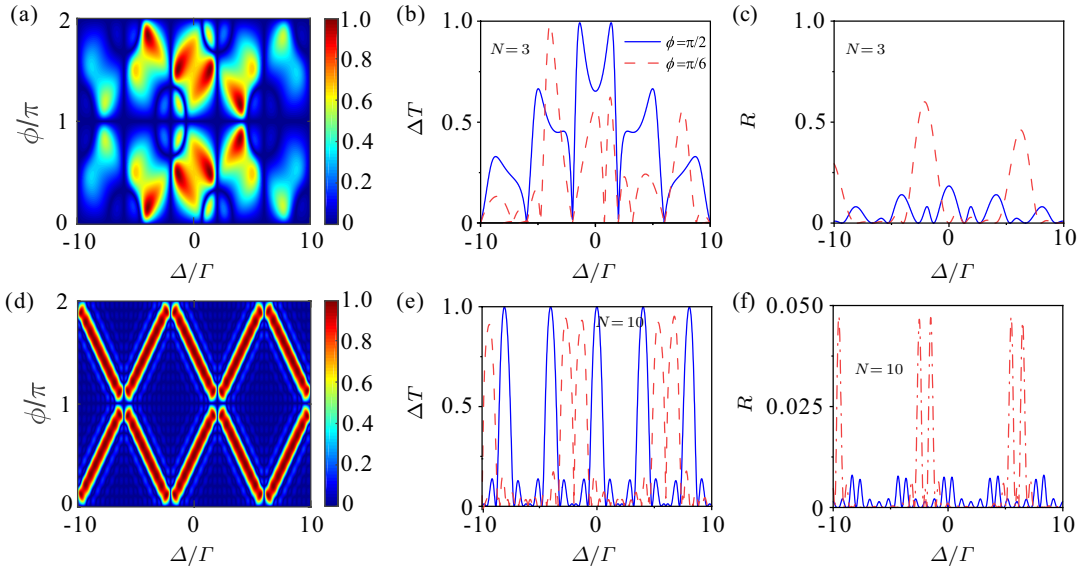


Fig. 5. ΔT varying with Δ and ϕ in the non-Markovian regime for $N = 3$ (a) and $N = 10$ (d). In the calculations, $\tau\Gamma = \pi/4$ and $\theta = \pi/2$. Panels (b) and (e) are extracted from (a) and (d), respectively, at $\phi = \pi/2$ and $\phi = \pi/6$. Panels (c) and (f) show the reflection spectra for $N = 3$ and $N = 10$, respectively. $\gamma = 2\Gamma$ is used in panel (a) and $\gamma = 50\Gamma$ in panel (d).

6. Discussion

In the previous sections, we assumed that all separations between coupling points were equal. In this part, we examine the influence of unequal separations. In this case, the parameters $\gamma_{\rm in}$, $\Delta_{\rm ls}$, and $\Gamma_{\rm eff}$ are given by

$$\gamma_{\rm in} = 2\Gamma \sum_{m>n}^{N} [\sin(\phi_m - \phi_n)\sin k(x_m - x_n)], \tag{20a}$$

$$\Delta_{\rm ls} = 2\Gamma \sum_{m>n}^{N} [\cos(\phi_m - \phi_n)\sin k(x_m - x_n)], \tag{20b}$$

$$\Gamma_{\rm eff} = N\Gamma + 2\Gamma \sum_{m>n}^{N} [\cos(\phi_m - \phi_n)\cos k(x_m - x_n)]. \tag{20c}$$

To illustrate the effects of unequal separations more clearly, we consider the three-point model as an example. As noted previously, when $\theta = \pi/2$, $\phi = (p \pm 1/6)\pi$, and $\gamma = 2\Gamma$, one obtains $\Delta T = 1$ at $\Delta = 2\sqrt{3}\Gamma$. Now, we set $\theta_1 = k(x_2 - x_1) = \theta - \Delta\theta$ and $\theta_2 = k(x_3 - x_2) = \theta + \Delta\theta$.

Figure 6 shows the influence of $\Delta\theta$ on ΔT. When $\Delta\theta$ is less than 0.1π, ΔT remains above 0.95. However, when $\Delta\theta$

reaches 0.2π, ΔT decreases to approximately 0.8. These results indicate that precise control of the separations is crucial for realizing quantum phenomena.

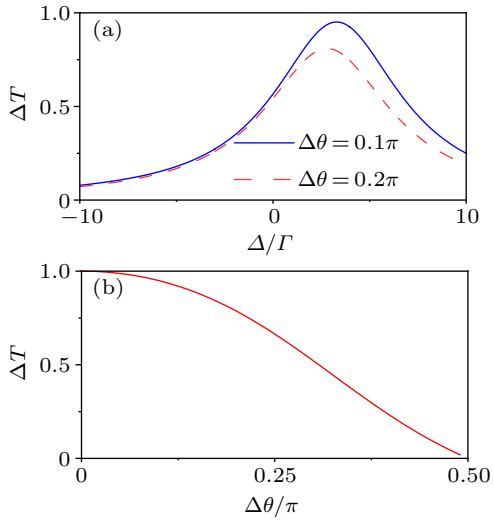


Fig. 6. ΔT varying with Δ for $\Delta\theta = 0.1\pi$ (blue solid line) and $\Delta\theta = 0.2\pi$ (red dashed line) in panel (a). ΔT as a function of $\Delta\theta$ at $\Delta = 2\sqrt{3}\Gamma$ is shown in panel (b). In the calculations, $N = 3$ and $\theta = \phi = \pi/2$.

7. Summary

We have investigated the single-photon scattering properties of a giant atom interacting with a waveguide at multiple coupling points. The phase differences between the coupling strengths play a crucial role in controlling the single-photon scattering properties, including the FWHM of the scattering spectra and the positions of the peaks. By adjusting these phase differences, the reflection spectra can be made superbroadened or subbroadened. The conditions for realizing perfect nonreciprocal single-photon transmission are presented for the multiple-point coupling model. When the decay of the giant atom is non-negligible, perfect nonreciprocal transmission can still be achieved by properly manipulating both the phase differences and the decay rate of the giant atom. In the non-Markovian regime, single-photon scattering spectra and nonreciprocal behavior can also be controlled through the phase differences of the coupling strengths. The results of this work may provide guidance for designing single-photon devices based on giant atoms.

Acknowledgments

This work is supported by the National Natural Science Foundation of China (Grant Nos. 12475010 and 119075023), the Major Project of the Natural Science Foundation of Anhui Provincial Department of Education (Grant No. 2022AH040053), and the Key Natural Scientific Research Projects of Universities in Anhui Province (Grant Nos. 2023AH051078 and 2023AH051125).

References

[1] Yang Y, Chapman R J, Youssry A, Haylock B, Lenzini F, Lobino M and Peruzzo A 2025 *npj Quant. Inf.* **11** 19
[2] Fang X X, Du H Y, Zhang X, Wang L, Chen F and Lu H 2025 *Laser Photon. Rev.* **19** 2400782
[3] Xing F, Lu Y and Liao Z 2022 *Opt. Express* **30** 22963
[4] Zheng H, Gauthier D J and Baranger H U 2013 *Phys. Rev. Lett.* **111** 090502
[5] González-Tudela A, Paulisch V, Kimble H J and Cirac J I 2017 *Phys. Rev. Lett.* **118** 213601
[6] Kim C M, Kim N C, Ko M C, Ryom J S, Ri S R and Ri J J 2024 *Quantum Inf. Process* **23** 394
[7] Song G Z, Guo J L, Liu Q, Wei H R and Long G L 2021 *Phys. Rev. A* **104** 012608
[8] Sheremet A S, Petrov M I, Iorsh I V, Poshakinskiy A V and Poddubny A N 2023 *Rev. Mod. Phys.* **95** 015002
[9] Jain K, Ruks L, Kien le F and Busch T 2024 *Phys. Rev. Res.* **6** 033311
[10] Scully M O and Zubairy M S 1997 *Quantum Optics* 1st edn. (Cambridge: Cambridge University Press)
[11] Xiang Z L, Ashhab S, You J Q and Nori F 2013 *Rev. Mod. Phys.* **85** 623
[12] Kannan B, Ruckriegel M J, Campbell D L, Frisk Kockum A, Braumüller J, Kim D K, Kjaergaard M, Krantz P, Melville A, Niedzielski B M and others 2020 *Nature* **583** 775
[13] Andersson G, Suri B, Guo L, Aref T and Delsing P 2019 *Nat. Phys.* **15** 1123
[14] Guo A L, Zhu L T, Guo G C, Lin Z R, Li C F and Tu T 2024 *Phys. Rev. A* **109** 033711
[15] Xu L and Guo L 2024 *New J. Phys.* **26** 013025
[16] Kuo P C, Lin J D, Huang Y C and Chen Y N 2023 *Opt. Express* **31** 42285
[17] Liu J Y, Jin J W, Liu H Y, Ming Y and Yang R C 2023 *Quantum Inf. Process* **22** 74
[18] Noachtar D D, Knörzer J and Jonsson R H 2022 *Phys. Rev. A* **106** 013702
[19] Wang X and Li H R 2022 *Quantum Sci. Technol.* **7** 035007
[20] Du L, Zhang Y, Wu J H, Kockum A F and Li Y 2022 *Phys. Rev. Lett.* **128** 223602
[21] Zou J P, Gong R Y and Xiang Z L 2022 *Front. Phys.* **10** 896827
[22] Zhang Y X, Carceller C R, Kjaergaard Mo and Sørensen A S 2021 *Phys. Rev. Lett.* **127** 233601
[23] Vadiraj A M, Ask A, McConkey T G, Nsanzineza I, Chang C W S, Kockum A F and Wilson C M 2021 *Phys. Rev. A* **103** 023710
[24] Kockum A F, Johansson G and Nori F 2018 *Phys. Rev. Lett.* **120** 140404
[25] Soro A and Kockum A F 2022 *Phys. Rev. A* **105** 023712
[26] Qiu Q Y, Zheng L L, Wu Y and Lü X Y 2025 *Laser Photon. Rev.* **19** 2401395
[27] Cai G, Lu Y, Ma X S, Cheng M T and Huang X 2021 *Phys. Rev. Lett.* **126** 043602
[28] Guo S, Wang Y, Purdy T and Taylor J 2020 *Phys. Rev. A* **102** 033706
[29] Frisk Kockum A, Delsing P and Johansson G 2014 *Phys. Rev. A* **90** 013837
[30] Zhao W and Wang Z 2020 *Phys. Rev. A* **101** 053855
[31] Zhao W, Tian T and Wang Z 2024 *Phys. Rev. A* **109** 063708
[32] Cai G, Lu Y, Liu Z, Cheng M T and Ma X S 2024 *Results Phys.* **57** 107381
[33] Ma X S, Quan J H, Lu Y N and Cheng M T 2024 *Eur. Phys. J. D* **78** 5
[34] Li X, Zhao W and Wang Z 2023 *Opt. Lett.* **48** 3595
[35] Zheng J C, Dong X L, Chen J Q, Hei X L, Pan X F, Yao X Y, Ren Y M, Qiao Y F and Li P B 2024 *Phys. Rev. A* **109** 063709
[36] Luo W B, Yin X L and Liao J Q 2024 *Adv. Quantum Technol.* **7** 2400030
[37] Wang D W, Zhao C, Yan Y T, Yang J, Wang Z and Zhou L 2024 *Phys. Rev. A* **109** 053720
[38] Cheng W, Wang Z and Liu Y X 2022 *Phys. Rev. A* **106** 033522
[39] Peng Y P and Jia W Z 2023 *Phys. Rev. A* **108** 043709
[40] Jia W Z and Yu M T 2024 *Opt. Express* **32** 9495
[41] Zhou J X, Zhu Z H, Zhang Y Q, Chen K K, Peng Z H, Chai Y F, Xiong Z Z and Tan L 2024 *Laser Phys. Lett.* **21** 055202
[42] Zhang Y Q, Zhu Z H, Chen K K, Peng Z H, Yin W J, Yang Y, Zhao Y Q, Lu Z Y, Chai Y F, Xiong Z Z and others 2022 *Front. Phys.* **10** 1054299
[43] Sun X J, Liu W X, Chen H and Li H R 2023 *Commun. Theo. Phys.* **75** 035103

[44] Cai Y, Ma K J, Liu J, Guo G F, Tan L and Liu W M 2024 *New J. Phys.* **26** 113003
[45] Chen Y T, Du L, Wang Z, Artoni M, La Rocca G C and Wu J H 2024 *Phys. Rev. A* **109** 063710
[46] Yang D C, Cheng M T, Ma X S, Xu J, Zhu C and Huang X S 2018 *Phys. Rev. A* **98** 063809
[47] Chen Y T, Du L, Guo L, Wang Z, Zhang Y, Li Y and Wu J H 2022 *Commun. Phys.* **5** 215
[48] Zhang X, Li H, Zeng R, Hu M, Xu M, Zhou X, Lan Y, Xia X, Xu J and Yang Y 2024 *Commun. Theo. Phys.* **76** 115501
[49] Chen K, Zhu Z, Zhang Y, Fu X, Peng Z, Lu Z, Chai Y, Xiong Z and Tan L 2024 *Laser Phys. Lett.* **21** 095203
[50] Zhou J, Yin X L and Liao J Q 2023 *Phys. Rev. A* **107** 063703
[51] Du L, Cai M R, Wu J H, Wang Z and Li Y 2021 *Phys. Rev. A* **103** 053701
[52] Li H, Zhang X, Zeng R, Hu M, Xu M, Zhou X, Xia X, Xu J and Yang Y 2024 *Opt. Express* **32** 38292
[53] Li S Y, Zhang Z Q, Du L, Li Y and Wu H 2024 *Phys. Rev. A* **109** 063703
[54] Liu N, Wang X, Wang X, Ma X S and Cheng M T 2022 *Opt. Express* **30** 23428
[55] Liu W, Lin Y, Li J and Wang X 2022 *Front. Phys.* **10** 894115
[56] Cai G, Lu Y, Ma X S, Cheng M T and Huang X 2023 *Opt. Express* **31** 33015
[57] Cai Q Y and Jia W Z 2021 *Phys. Rev. A* **104** 033710
[58] Liu J, Cai Y, Ma K J, Tan L and Liu W M 2024 *Phys. Scr.* **99** 105119
[59] Xu L and Guo L 2025 arXiv:2502.08156 [hep-ph]